ELSEVIER

Polymer 44 (2003) 2761–2772

polymer

www.elsevier.com/locate/polymer

Polyamide-12 layered silicate nanocomposites by melt blending

Tony McNally[a,*], W. Raymond Murphy[b], Chun Y. Lew[b], Robert J. Turner[c], Gerard P. Brennan[d]

[a]*Materials Research Group, School of Mechanical and Manufacturing Engineering, Queen's University Belfast, Belfast BT9 5AH, UK*
[b]*Polymer Processing Research Centre, Queen's University Belfast, Belfast BT9 5AH, UK*
[c]*School of Mathematics and Physics, Condensed Matter Physics and Materials Science Division, Queen's University Belfast, Belfast BT7 1NN, UK*
[d]*School of Biology and Biochemistry, Medical Biology Centre, Queen's University Belfast, Belfast BT9 7BL, UK*

Received 5 November 2002; received in revised form 10 February 2003; accepted 13 February 2003

Abstract

Polyamide-12/tetrasilisic fluoromica (PA12-ME100) and polyamide-12/quaternary tallow ammonium chloride modified fluoromica nanocomposites (PA12-MAE) were prepared by melt compounding. The nanocomposite morphology and clay dispersion were investigated using wide angle X-ray diffraction (XRD), scanning electron microscopy (SEM), SEM-energy dispersive X-ray analysis (SEM-EDX), transmission electron miscroscopy (TEM), high resolution transmission electron microscopy (HRTEM) and atomic force microscopy (AFM). A predominantly intercalated morphology was observed for PA12-ME100, and a very high degree of exfoliation for PA12-MAE. HRTEM showed that the polymer crystallites lie perpendicular to the clay surface. The tensile and flexural properties of the PA12-MAE nanocomposite were significantly enhanced compared to neat polyamide-12, even with the addition of only 4 wt% nanoclay. Furthermore, the elongation at break (%) increased from 180% for polyamide-12 up to >500% for the PA12-MAE nanocomposite. In situ measurement of the heat generated in the test specimens during uniaxial tensile deformation using infra-red thermal imaging showed that the temperature of the dumbbell samples increased from room temperature (23 °C) to as high as 70 °C regardless of the strain rate used. This is considerably above the glass transition temperature (T_g) of PA12-MAE (30 °C), as measured by dynamic mechanical thermal analysis (DMTA). The mechanism of deformation is partially explained in terms of microvoid formation. The shear viscosity of the PA12-MAE nanocomposite determined by dual capillary rheometry was lower than both neat polyamide-12 and PA12-ME100. The reduction in shear viscosity of the nanocomposites was shown, from gel permeation chromatography (GPC) studies, not to originate from polymer degradation during melt blending. The coefficient of thermal expansion, decomposition temperature, and melting and crystallisation temperatures and relative crystalline content of the nanocomposite materials were measured by thermo-mechanical analysis (TMA), thermogravimetric analysis (TGA) and differential scanning calorimetry (DSC) respectively—properties which can be related to polymer nanoclay interactions.

Keywords: Polyamide-12; Layered silicates; Melt blending

1. Introduction

Polymer nanocomposites constitute a new class of materials that are hybrid structures between an organic phase (the polymer) and an inorganic phase (a layered silicate), where the inorganic component has at least one dimension on a nanometer scale. Nanocomposites have been known about for over 50 years [1], the first polyamide based nanocomposite being reported in 1976 [2]. However, it was the introduction by the Toyota Motor Company of a timing belt cover in 1988 [3] made using a polyamide-6 nanocomposite [4,5] that has stimulated the present intense research effort worldwide.

The layered silicates used in nanocomposites belong chemically to the family known as the 2:1 phyllosilicates, such as mica, talc, montmorillonite and hectorite [6]. The layer thickness is typically 1 nm with the lateral dimensions of the layers varying between 20 nm and tens of microns depending on the source of the clay. The layers are stacked and separated by a van der Walls gap, known as the interlayer, gallery or interstratum. Isomorphous substitution within the silicate layers generates a net negative charge on the layer, which is delocalised around neighbouring oxygen atoms [7,8]. Cationic exchange between the layers can be readily achieved with surfactants such as primary, tertiary and quaternary ammonium or phosphonium ions, which

* Corresponding author. Tel.: +44-28-902-747-12; fax: +44-28-906-617-29.
E-mail address: t.mcnally@qub.ac.uk (T. McNally).

0032-3861/03/$ - see front matter © 2003 Elsevier Science Ltd. All rights reserved.
doi:10.1016/S0032-3861(03)00170-8

make the normally hydrophilic silicate surface organophilic. If favourable interactions exist between the polymer and layered silicate the organic and inorganic phases will be dispersed on the nanometer scale. Consequently, polymer layered nanocomposites exhibit unique properties not seen for conventionally filled polymers. Two idealised and somewhat simplified polymer layered silicate nanoscale morphologies are postulated, intercalated and exfoliated. Intercalated structures result when a polymer chain has diffused into the interlayer space and an expanded ordered multilayer is obtained. Exfoliated structures are achieved when individual nanometer thick layers are dispersed throughout the polymer matrix. More recently Vaia et al. introduced the concept of ordered and disordered intercalated and exfoliated structures [9,10].

There are at least three experimentally proven methods to fabricate polymer layered silicate nanocomposites. The first, known as solution mediated processing or solvent mixing, involves the use of a solvent to disperse the organophilic layered silicate as well as the polymer [11–17]. Uniform mixing of the polymer and layered silicate is achieved upon removal of the solvent. The structure of the nanocomposite obtained depends on molecular factors such as intermolecular interactions and surface energies, and kinetic factors such as solvent evaporation rate and shear mixing. This technique in particular has been widely used with water soluble polymers to produce intercalated polymers based on poly(vinyl alcohol) [18], poly(ethylene oxide) [19,20] and poly(acrylic acid) [21]. Polymer intercalation can also occur in organic solvents. Poly(ethylene oxide) has been successfully intercalated in sodium montmorillonite and sodium hectorite by solution blending in acetonitrile [22]. High density polyethylene nanocomposite has been made using a similar process where the polyethylene chains were dissolved in a 80:20 wt% xylene and benzonitrile with 20 wt% modified clay [23]. The second method for preparing polymer nanocomposites is in situ polymerisation [24–27]. A monomer is polymerised after absorption into the interlayer space of the clay. Numerous mono- and multifunctional monomers have been studied yielding a linear or cross-linked polymer matrix. Akelah and Moet [28] successfully made polystyrene nanocomposites by dispersing vinylbenzyl-trimethyl ammonium chloride modified sodium and calcium montmorillonite in various solvents in the presence of an initiator. More recently Zeng and Lee polymerised methyl methacrylate and styrene in the presence of dimethyl dihydrogenated tallow ammonium montmorillonite [29]. Both intercalated and exfoliated structures have been obtained for PMMA nanocomposites synthesised by suspension and emulsion polymerisation [30,31].

The final fabrication process, first reported by Vaia et al. in 1993 involves mixing the layered silicate with the polymer in the molten state above its softening point [32]. Shear flows encountered using conventional compounding equipment facilitate mixing of the polymer and clay and control the alignment of the layers. Melt intercalation of polystyrene and its derivatives have been studied using this technique. Vaia and Giannelis studied polystyrene as the polymer matrix for dispersing different types of unmodified and modified clays [33]. Kato et al. reported the melt intercalation of polypropylene modified with either maleic anhydride (PP-MA) or hydroxyl groups (PP-OH) in octadecylammonium modified montmorillonite [34]. Several other polymer nanocomposites have been prepared using this method, including ethylene vinyl acetate copolymers [35], styrene/butadiene/styrene block copolymers [36], various elastomers [37,38], polyethlene [39], polypropylene [40,41], polyamide-6 [42] and polylactide [43]. The melt blending method of fabrication is much more commercially attractive than the former two methods, as both solvent processing and in situ polymerisation are less versatile and environmentally contentious.

In this paper we report the preparation of polyamide-12 nanocomposites by melt blending. We discuss the effect clay surface modification has on composite properties. We examine the morphological structures obtained and the extent of dispersion of the nanoclay in the polymer matrix using XRD and a range of microscopic techniques. We relate the differences in mechanical, rheological, thermal and thermo-mechanical properties of the nanocomposites compared to neat polyamide-12 with nanocomposite morphology and polymer clay interactions.

2. Experimental

2.1. Materials

Polyamide-12 (Grilamid L25W40X natural, $M_w = 126,000$, $M_n = 72,200$, polydispersity $= 1.8$) was obtained in pellet form from EMS-CHEMIE AG, Switzerland. This is a plasticised grade used in automotive fluid handling applications. Two synthetic clays, SOMASIF ME100 and MAE, grades provided by CO-OP Chemical Co. of Japan, and based on a three layer tetrasilisic fluoromica were melt compounded with the polyamide-12. The SOMASIF clays were synthesised by heating talc and Na_2SiF_6 for several hours in an electric furnace. However, the surface of the MAE clay was modified to be more organophilic by means of ion exchange with quaternary tallow ammonium chloride. The amount of organic modifier, tallow, on the clay was 43% by weight and had the following composition: C_{16}—74%; $C_{18\ saturated}$—24%; $C_{18\ unsaturated}$—1%.

2.2. Preparation of polyamide-12 nanocomposites

Polyamide-12 in pellet form was first cryogenically ground to a powder, using a Wedco horizontal single stage grinding mill. The powder after sieve analysis (BS 410) was found to have an average particle size of 260 μm. The powder was then dried at 80 °C for 24 h in a dehumidifying

dryer before being tumble mixed with 4 wt% of ME100 or MAE clay powder prior to melt compounding. The nanocomposites were prepared by melt blending the components in a Killion KN150 38 mm diameter 30:1 L:D single screw extruder fitted with a barrier mixing screw having a spiral Maddock mixing zone. The die temperature was maintained at 225 °C and the nanocomposites prepared using several screw speeds between 15 and 45 rpm. The properties of the materials made at 25 rpm, hereafter abbreviated to PA12-ME100 and PA12-MAE are reported in this paper. The effect of processing variables on the nanocomposite properties will be discussed in detail in a future publication. The PA12-ME100 blend was passed through the extruder twice, the PA12-MAE blend once, to optimise the mixing of the components. Nanocomposite extrudates were thereafter cooled in a water bath at room temperature (21 °C) and pelletised.

2.3. Characterisation of nanocomposite morphology

The wide-angle X-ray diffraction (XRD) spectra of samples taken from injection moulded test specimens (normal to the flow direction) of pristine polyamide-12 and the nanocomposites were recorded using a Siemens D5000 diffractometer using Cu Kα radiation ($\lambda = 1.5406$ Å) at a scanning rate of 0.3 °/min. over the range 2–60 2theta. The dispersion of the clays on a microscopic scale was examined using a JOEL 6400 scanning electron microscope (SEM) and an operating voltage of 15 kV. Samples were taken from cryofractured tensile dumbbell specimens perpendicular to the injection flow direction, dried and gold coated. The chemical composition of the dispersed clay phase was measured using a JOEL 733 Superprobe X-ray microanalyser, sensitive to 200 ppm ± 1%. Similar to the SEM study, samples were taken normal to the injection flow from tensile dumbbell specimens, but in this instance the surface was carbon coated. The nanoscale morphology of the nanocomposites was investigated by transmission electron microscopy (TEM), high resolution transmission electron microscopy (HRTEM) and atomic force microscopy (AFM). TEM was performed with a Phillips CM100 instrument using an accelerating voltage of 100 kV on ultra-thin samples (typically 60 nm) microtomed from moulded test pieces (perpendicular to the injection flow direction), using an Ultracut-E Reichert Jung ultramicrotome. HRTEM was carried out using a FEI Tecnai F20 field emmision instrument on similarly microtomed samples which were then stained following the procedure described by Weber et al. [44]. AFM studies were performed on ultramicrotomed samples using a Digital Instruments Nanoscope 111a model in the phase mode. Force modulation SPM tips were used. The tip was mounted on a 225 μm (length), 3 μm (thickness) single beam cantilever with resonant frequencies of 75 kHz and a force constant of 2.8 N/m. The tip height was in the range 10–15 μm with a sharp edge of 10 nm.

2.4. Mechanical, flexural and impact property measurement

Tensile, flexural and impact test specimens were moulded using an Arburg 320S Allrounder 500-350 injection moulding machine having a screw diameter of 45 mm and L:D ratio of 18:1 at 240 °C with a holding pressure of 25 bar. The tensile modulus and strength were measured using an Instron 4411 Universal Tester (ASTM D 638M) at crosshead speeds between 50 and 200 mm/min. The flexural modulus and strength were determined using the same Instron instrument but in a 3-point loading test (ASTM 790M) using a crosshead speed of 5 mm/min. and a specimen length to depth ratio of 32:1. Two-dimensional impact testing at room temperature and −40 °C of the polymer nanocomposites was performed using a CEAST Fractovis instrumented free falling dart test (ASTM D5628) fitted with WIN DAS 4000 data acquisition system and using a falling load of 28.63 kN. The frictional heat generated in the dumbbell test pieces during tensile testing was measured using an Infrared-thermal imaging system. The temperature profile of the sample was obtained in situ and digitised using an AGEMA Thermovision 900 infrared system fitted with a 20′LW193322 IR lens. The effect of the modified clay on the glass transition temperature of polyamide-12 was monitored by dynamic mechanical thermal analysis (DMTA). Measurements were made using a Rheometric Scientific DMTA V instrument at six different frequencies, 0.1, 0.3, 1, 10, 30 and 100 Hz. in the dual cantilever mode over the temperature range −50–100 °C at a strain rate of 0.005%. Activation energies were calculated using an Arrhenius type expression.

2.5. Rheological analysis

The rheological behaviour of the nanocomposites was examined using a Rosand Precision Advanced dual capillary extrusion rheometer. Measurements were made at 16 different shear rates between 10 and 1000 s^{-1} at 220 °C. The data collected was Bagely corrected for end and exit effects from the die [45].

2.6. Molecular weight distribution (MWD)

MWD was characterised using Gel Permeation Chromatography (GPC). PA12, PA12-ME100 and PA12-MAE were first made up in a 50:50 (w/w) trichlorobenzene:phenol solution. GPC measurements were performed using a Polymer Laboratories GPC-210 instrument with a PL gel2 column, using a refractive index detector and operated at 115 °C. Subsequent data acquisition and computation of the results was carried out using Viscotek Trisec 3.0 software.

2.7. Thermal analysis

Differential scanning calorimetry (DSC) was employed to investigate the effect of the clay on the melting and crystallisation behaviour of polyamide-12. Samples of neat polyamide-12, PA12-ME100 and PA12-MAE were studied using a Perkin–Elmer DSC model 6 using a heating and cooling rate of 10 °C/min between 30 and 240 °C under an inert nitrogen atmosphere. In all cases the samples were held at 240 °C for 5 min prior to cooling to remove previous thermal history. The samples were then cooled to 30 °C at 10 °C/min. and reheated again to 240 °C at 10 °C/min. The coefficient of thermal expansion of neat polyamide-12, PA12-ME100 and PA12-MAE was measured by thermal mechanical analysis (TMA) with a Perkin Elmer TMA model 7 using a static force of 110 kN. The measurements were performed on samples taken from injection moulded test specimens normal to the flow direction, and were scanned over the range 25–140 °C at a heating rate of 2 °C/min. The thermal stability and the inorganic clay content of the nanocomposites were determined using thermogravimetric analysis (TGA). TGA measurements were performed using a TA Instrument, Hi-Res TGA 2950 thermogravimetric analyser from 25 to 550 °C with a heating rate of 10 °C/min. and nitrogen gas flow rate of 40/60 cm^3/min.

3. Results and discussion

Fig. 1 shows the XRD patterns for neat polyamide-12, the unmodified ME100 clay, the tallow modified MAE clay, PA12-ME100 and PA12-MAE. The interlayer spacing of the materials was calculated from the d_{001} basal reflection peak positions using the Bragg equation, and both sets of values are listed in Table 1. The ME100 pattern contains five peaks between $2\theta = 7.1$ and 28.8° ($d_{001} = 1.24$ and 0.31 nm). The mean interlayer spacing was about 0.96 nm and is similar to that reported previously by other workers [46,47]. In contrast, the XRD pattern of the quaternary alkylammonium modified MAE clay revealed some 10 peak positions between $2\theta = 2.6$ and 27.7° ($d_{001} = 3.40$ and 0.32 nm), indicating that the interlayer spacing of the silicate stacks had been significantly swollen from 1.24 to 3.40 nm as a consequence of the cationic exchange reaction, and mainly due to the presence of alkyl (C_{16} to C_{18}) chains. The XRD pattern for polyamide-12 itself shows one large peak at $2\theta = 21°$ and is derived from the stable γ-crystal phase of polyamide-12 [48,49]. The XRD pattern for PA12-ME100 shows four peaks all shifted to slightly lower 2θ positions, and the peak at 7.1° observed for ME100 alone has disappeared. This behaviour is associated with an intercalated hybrid structure. Also, the intensity of the peaks associated with the clay structure were more intense for PA12-ME100 compared to ME100 alone. The increased intensity of these peaks may be derived from orientation effects as a consequence of the injection moulding process. The diffraction pattern obtained for PA12-MAE showed only four clearly resolved peaks. The one associated with

Table 1
WAXD characteristics of PA12, pristine clays and PA12 nanocomposites

PA12 2θ (d_{001}, nm)	ME100 2θ (d_{001}, nm)	PA12-ME100 2θ (d_{001}, nm)	MAE 2θ (d_{001}, nm)	PA12-MAE 2θ (d_{001}, nm)
21 (0.43)	7.1 (1.24)	Exfoliated	2.6 (3.40)	–
	9.2 (0.96)	8.9 (0.99)	4.2 (2.10)	4.1 (2.15)
	18.6 (0.48)	18.2 (0.49)	5.6 (1.58)	–
	28.0 (0.32)	21.0 (0.43)	7.2 (1.25)	6.2 (1.42)
	28.8 (0.31)	26.0 (0.34)	10.0 (0.88)	8.2 (1.08)
			17.4 (0.51)	Exfoliated
			19.4 (0.46)	Exfoliated
			22.5 (0.40)	Exfoliated
			24.8 (0.36)	Exfoliated
			27.7 (0.32)	Exfoliated

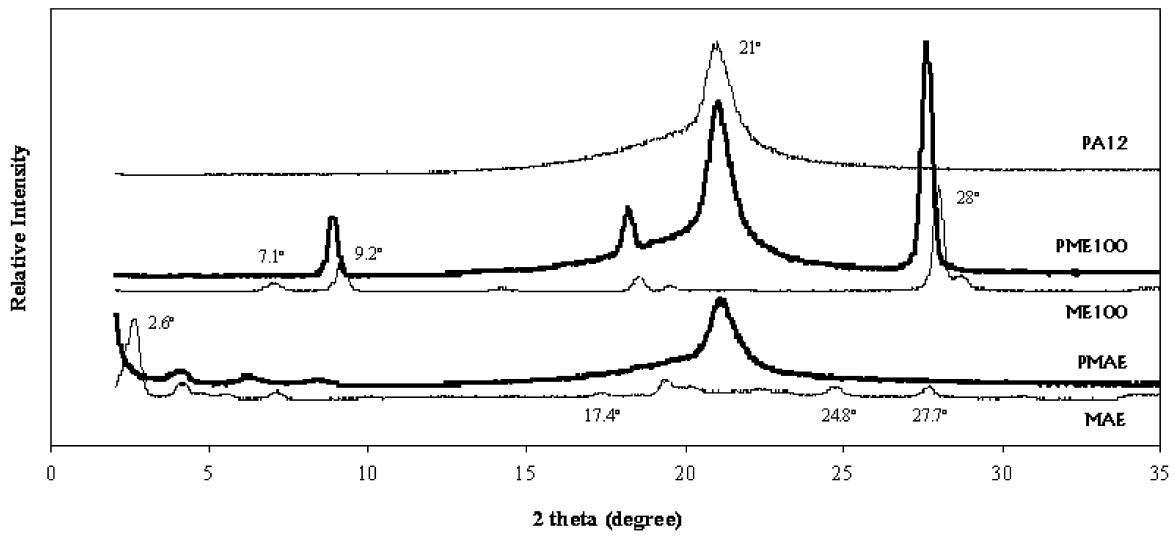

Fig. 1. Wide angle X-ray diffraction patterns for PA12, ME100, MAE, PA12-ME100 and PA12-MAE.

the crystalline phase of polyamide-12 ($2\theta = 21°$) was less intense than that obtained for neat polyamide-12. There is some evidence of a peak below that observed at $2\theta = 2.6°$ for MAE alone, which is outside the measurement capabilities of the instrument used. The absence of peaks seen previously in the pattern for pristine MAE would imply that the PA12-MAE contains both exfoliated and intercalated structures. The crystalline content of PA12, PA12-ME100 and PA12-MAE was calculated by integrating the areas attributed to the crystalline and amorphous scattering, and revealed that the fraction of polyamide-12 phase that crystallised increased by about 6% for PA12-ME100, but decreased by 36% for PA12-MAE. The presence of the dispersed silicate layers hinders the incorporation of polymer chains into lamellae structures and thus retards crystallite growth. The trends observed from XRD are in reasonable agreement with those determined from DSC measurements and will be discussed later.

The effect of processing conditions on the dispersion of the unmodified ME100 in polyamide-12 was examined. Fig. 2(a) and (b) show the SEM micrographs of PA12-ME100 after one and two passes through the blender. The dispersion of the clay tactoids is not uniform, but is improved after a second stage melt blending. The lateral dimensions of the tactoids decreased from about 2 μm to 200 nm. In complete contrast, for PA12-MAE, see Fig. 2(c) and (d), the MAE clay is uniformly dispersed throughout the PA12 matrix. SEM-EDX analysis was performed on samples for both PA12-ME100 and PA12-MAE. Elemental analysis of a random sample of the particles seen in the electron micrographs showed these areas to be highly enriched in silicon, and to a lesser extent magnesium and sodium, and as such we deemed these particles to be tactoids. Sulphur was also detected in the tactoids. The polyamide-12 used in this study was plasticised with *n*-butylbenzene sulphonamide, which thus would indicate that either the plasticiser alone or plasticiser and polymer chains have diffused into the interlayer space, giving rise to the intercalated structures detected by XRD.

Micro- and nanostructural characterisation was also performed using conventional and high-resolution transmission electron microscopy. Fig. 3(a) shows a TEM of PA12-ME100 tactoids having lateral dimensions typically between 200 and 500 nm, in good agreement with those seen in the micrographs obtained by SEM. The TEM micrograph in Fig. 3(b) of PA12-MAE clearly shows exfoliated structures. This was further confirmed when PA12-MAE was studied using HRTEM, Fig. 3(c), where individual clay platelets are randomly distributed in the polyamide-12 matrix. Furthermore, HRTEM revealed that

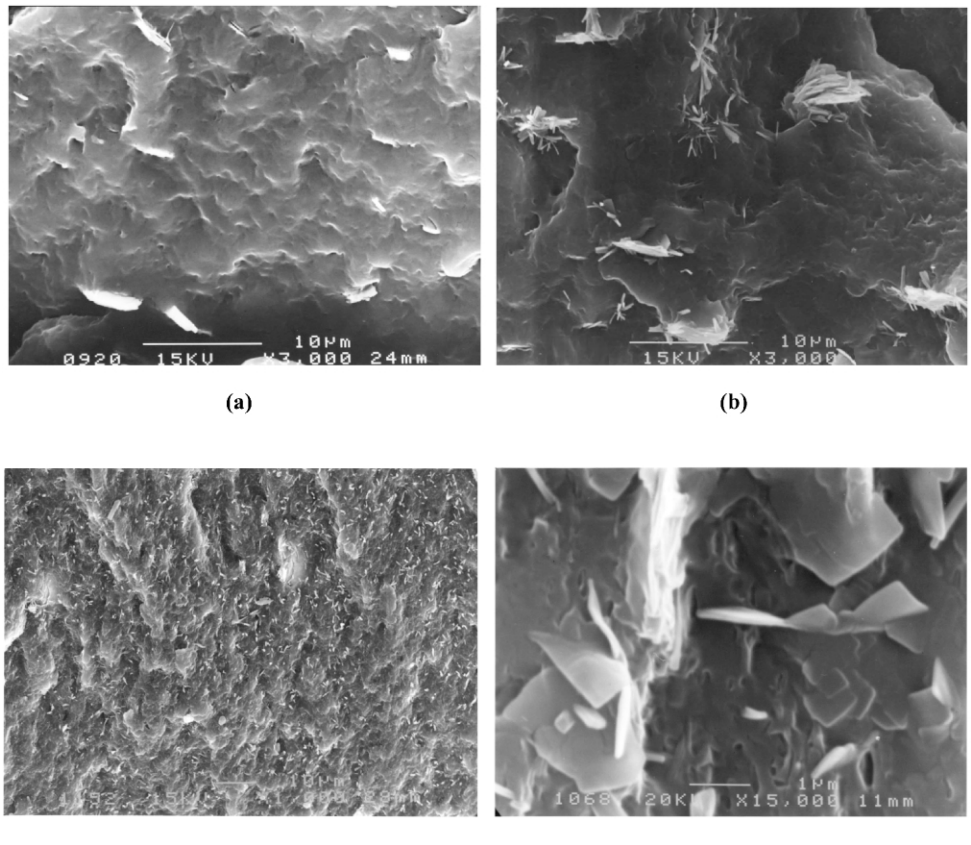

Fig. 2. Scanning electron micrographs (SEM) of (a) PA12-ME100; single pass in compounder, (b) PA12-ME100; double pass in compounder, (c) PA12-MAE; showing extent of dispersion and (d) PA12-MAE; showing tactoid dimensions.

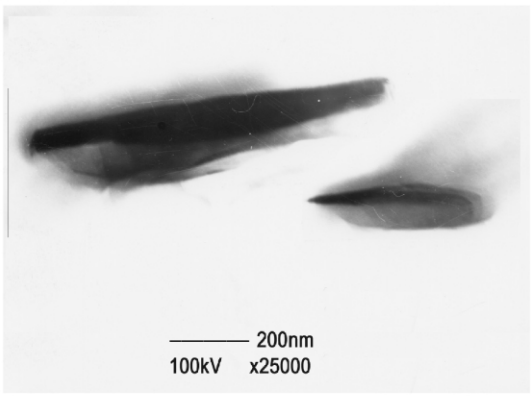

(a)

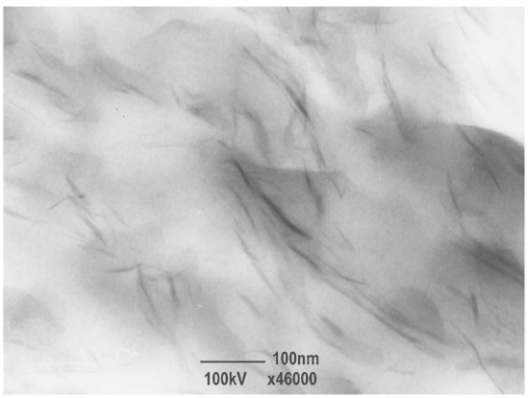

(b)

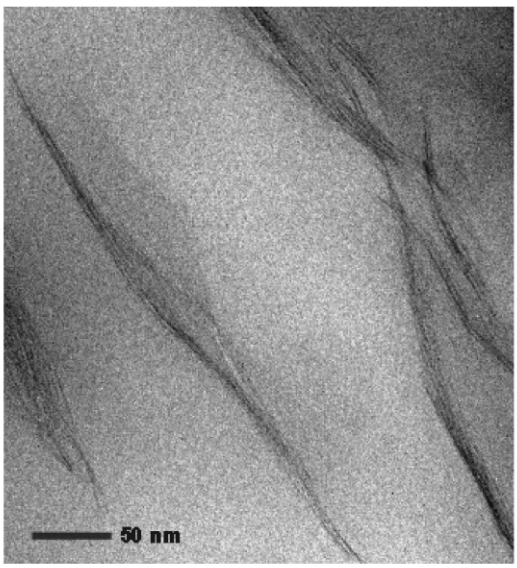

(c)

Fig. 3. Transmission electron micrographs [TEM] of (a) PA12-ME100 tactoids, (b) PA12-MAE; showing excellent delamination and dispersion and (c) a high resolution transmission electron micrograph [HRTEM] of PA12-MAE showing single platelet layers.

the PA12 crystallites lie perpendicular to the injection moulding direction. This phenomenon has some bearing on the mechanical properties measured and will be discussed later in this paper. The atomic force images shown in Fig. 4(a) and (b) for PA12-ME100 also showed average tactoid dimensions in the order of a few hundred of nanometers. The AFM image in Fig. 4(c) shows the top surface of a platelet for PA12-MAE, and in Fig. 4(d) the extent of the dispersion of MAE platelets in the polyamide-12 matrix is evident.

The mechanical and impact properties measured for pristine polyamide-12, PA12-ME100 and PA12-MAE are listed in Table 2. The tensile strength of PA12-ME100 was similar to neat polyamide-12, but the tensile strength of PA12-MAE was about 50% greater than polyamide-12 itself. A similar trend was obtained for tensile modulus, the value obtained for PA12-MAE was 27% greater than that for PA12 itself. However, the tensile modulus of PA12-ME100 was also greater by about 11% compared to PA12 alone. The most striking property enhancement was observed when the elongation at break was measured. The average value obtained for the PA12 studied, a highly plasticised (~14%) grade, was 182%. The value measured for PA12-MAE was in excess of 500% and approximately half of the test specimens examined did not fail during the test. Those samples that did not fail also recovered elastically by between 20 and 30%. In contrast, the elongation at break for the composite containing the unmodified clay fell slightly by 5%.

Significant heat was generated during tensile testing of the PA12-MAE, irrespective of the strain rate used. The heat generated during testing for PA12 alone and PA12-MAE was measured using infra-red thermal imaging. Fig. 5 shows the heat build up for both samples immediately before and just after failure during testing. For PA12 itself, the temperature of the sample increased from room temperature (23 °C) to typically 33 °C along the length of the sample with the exception of the point of failure. However, the temperature increase measured for PA12-MAE during testing was significant, increasing from 23 °C to as high as 70 °C for several test specimens. This 47 °C rise in temperature was obtained for all PA12-MAE tests at strain rates between 5 and 200 mm/min. While there will be a contribution to this heat build-up

Table 2
Mechanical and impact properties of PA12 and PA12 nanocomposites

Property	PA12	PA12-ME100	PA12-MAE
Tensile strength (MPa)	32.2	32.0	48.2
Tensile modulus (MPa)	177	197	224
Elongation at break (%)	182	173	>500
Flexural strength (MPa)	11.2	11.5	12.5
Flexural modulus (MPa)	378	459	570
Impact strength; 23 °C (J/mm)	14.5	14.0	13.4
Impact strength; −40 °C (J/mm)	17.7	8.3	1.7

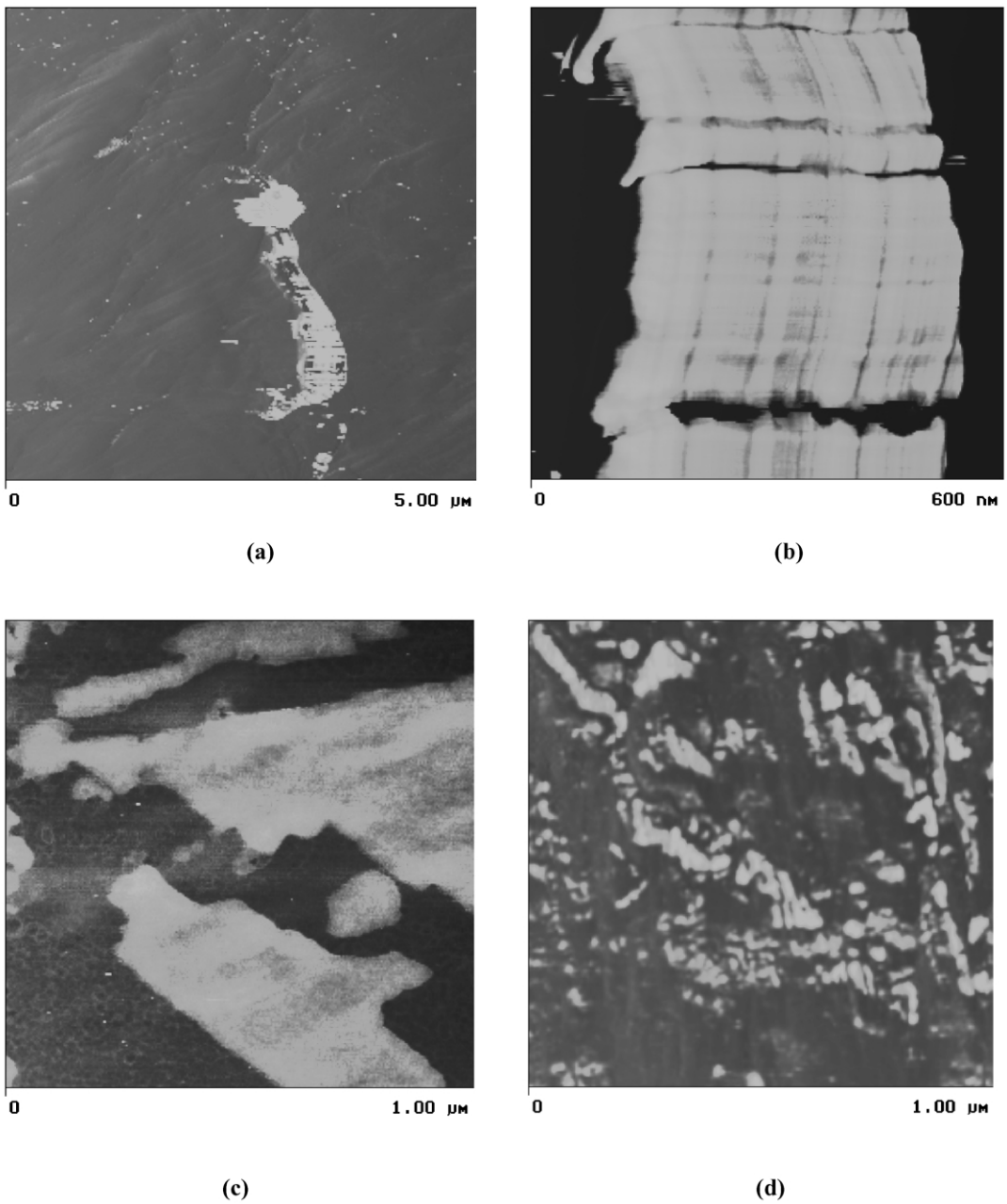

Fig. 4. Atomic force microscope images of (a) and (b) PA12-ME100 (second pass); showing dimensions of tactoid and the layer stacking of platelets to 500 nm respectively, (c) PA12-MAE; showing top surface of tactoids and (d) PA12-MAE; showing extent of dispersion of clay platelets.

from adiabatic heating, it could not account for all 47 °C rise. The presence of the nanofiller and its orientation, together with the orientation of the PA12 crystallites perpendicular to the injection moulding direction permit the test piece to maintain its integrity during deformation for longer than neat PA12. The nanocomposite can efficiently dissipate the internal friction generated as heat. This is achievable for three reasons, firstly due to microvoid formation, which permits heat dissipation by deformation mechanisms. Secondly, by transfer of energy from clay layers bonded to polymer crystallites, and thirdly by the splitting, opening and sliding of clay stacks. Kim et al. studied the deformation mechanism for a PA12-ME100 system in situ in an electron microscope, and proposed a similar deformation process [47]. However, the larger interlayer spacing of the MAE clay compared to ME100 (3.4 nm as opposed to 0.95 nm) will have a significant effect on microvoid formation, as will the presence of polymer chains in the interlayer spacing and any interactions that may occur between the modified clay surface and the polar polyamide-12. The combination of improved stiffness, strength and toughness obtained for PA12-MAE is due to the load bearing and microvoid formation ability of the nanofiller, and the

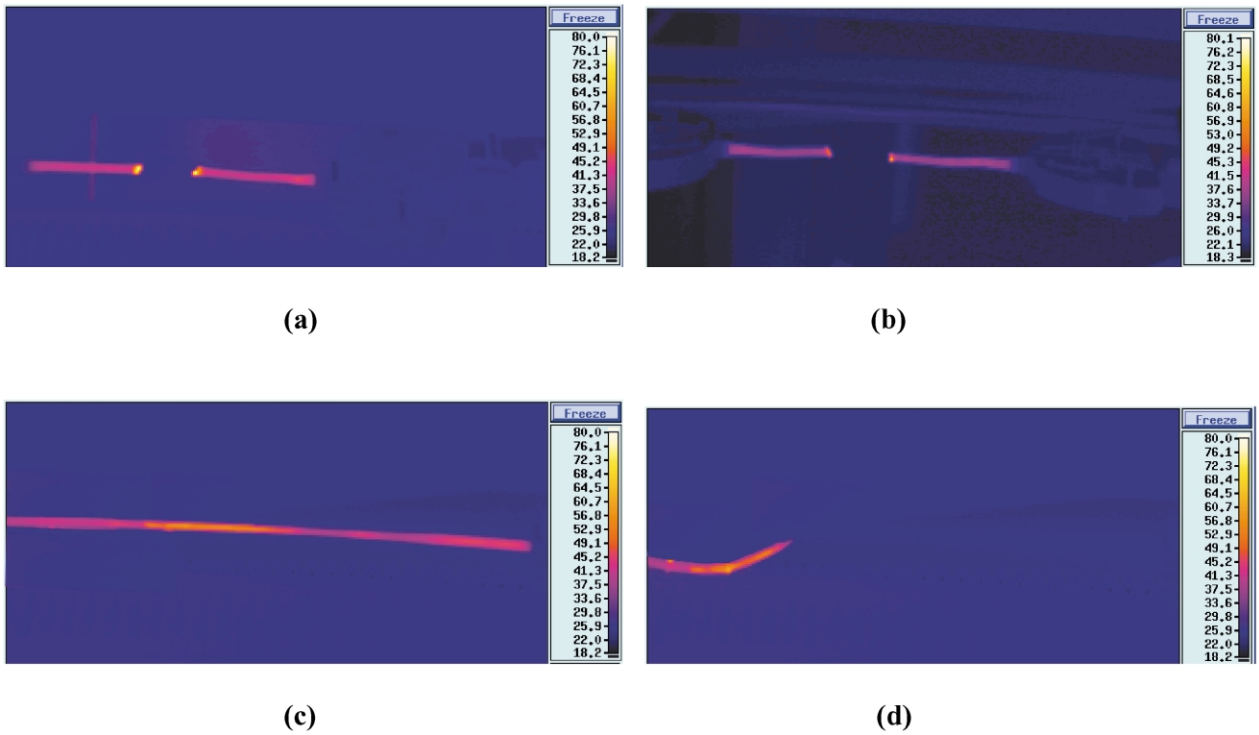

Fig. 5. Infra-red thermal images obtained just before and immediately after failure during tensile testing of (a) and (b) PA12, and (c) and (d) PA12-MAE.

effect the nanoclay has on the crystalline morphology of the polyamide-12 matrix.

As the temperature of the PA12-MAE sample rises during tensile testing, the nanocomposite goes through its glass transition process. The nanocomposite thus behaves 'elastomeric', reflected by a significant increase in the value of elongation at break and the observed recovery of the test specimens. This is a surprising result, given that even the addition of 4 wt% of an inorganic nanofiller to a semicrystalline polymer such as polyamide-12 should produce a material exhibiting such behaviour. This behaviour may be important for improved fire retardant properties.

Small improvements in flexural strength for PA12-ME100 (2.7%) and PA12-MAE (11.6%) over pristine polyamide-12 were achieved. But significant enhancements in flexural modulus for both composite materials were obtained. The flexural moduli of PA12-ME100 and PA12-MAE were respectively 21 and 50% greater than that for polyamide-12 alone. A slight deterioration in the room temperature impact (23 °C) strength for both PA12-ME100 and PA12-MAE was recorded, falling from 14.5 J/mm for PA12 to 14.0 J/mm for PA12-ME100 to 13.4 J/mm for PA12-MAE, a drop of 7.5%. In contrast, the cold temperature (−40 °C) impact properties of both composite materials were much poorer than the polymer itself. The −40 °C impact strength of PA12-ME100 fell by 47% compared to PA12, but the fall in impact strength at −40 °C for PA12-MAE was most catastrophic, dropping by as much as 90%. We associate, in part, the poor cold temperature impact properties of the PA12-MAE nanocomposite with the 'freezing-in' of the brittle C_{16}–C_{18} 'wax-like' modified surface of the MAE clay.

The rheological properties of polyamide-12, PA12-ME100 and PA12-MAE were measured using dual capillary rheometry. Fig. 6 shows a plot of shear viscosity for all three materials as a function of shear rate. The shear rate range examined, between 10 and 1000 s^{-1} covers the shear experienced during most polymer processing techniques. The viscosity of the PA12-ME100 was greater than that of neat PA12 in the shear rate range 10–400 s^{-1}, and then merged with that of PA12 between 400 and 1000 s^{-1}. The

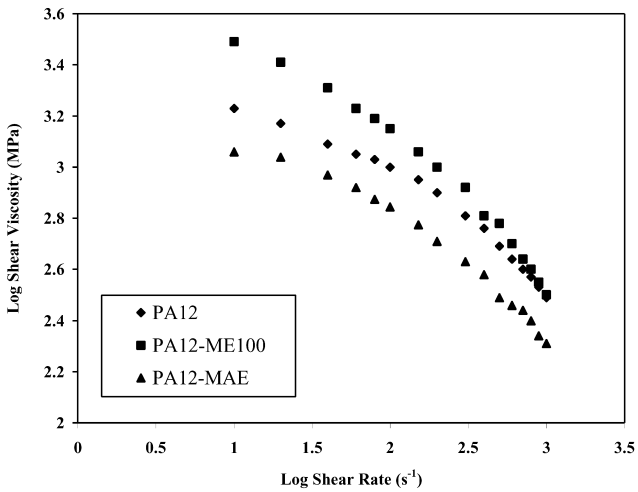

Fig. 6. Influence of clay type on the apparent shear viscosity of PA12 as a function of shear rate.

viscosity of the PA12-MAE nanocomposite over the entire shear rate range was lower, by about one third, than the polyamide-12 and significantly lower than the PA12-ME100 composite. The lower viscosity of the nanocomposite would imply that it could be more easily melt processed. Paul et al. reported similar results for a polyamide-6 bis(hydroxyethyl) (methyl) rapeseed alkyl ammonium chloride modified sodium montmorillonite nanocomposite [50]. The lower viscosity in the molten state may be associated with the slippage of polymer chains over the nanoclay platelets or as has been suggest by a number of workers due to molecular weight reduction as a result of degradation and chain scission of the polymer matrix during melt compounding [43,47].

We tested this latter hypothesis by measuring the molecular weight distribution (MWD) of all three materials by GPC. Fig. 7 shows the gel permeation chromatographs, in duplicate, for the as received PA12, and for PA12-ME100 and PA12-MAE samples taken from their extrudate. No change in the molecular weight distribution (M_w) of polyamide-12 was detected on addition of either the ME100 or MAE clays to neat polyamide-12. GPC characterisation was also performed on samples of all three materials taken from injection moulding test specimens. No variation in molecular weight distribution was seen for the PA12-MAE nanocomposite compared to polyamide-12. However, the maximum in MWD of the PA12-ME100 composite, irrespective of whether it had one or two passes in the blender had fallen by some 20%. In some way the more poorly dispersed, unmodified ME100 clay initiates degradation of the polyamide-12 matrix during a second or third thermal and shear cycle experienced during injection moulding.

DSC, TGA and TMA were performed on polyamide-12, PA12-ME100 and PA12-MAE and a summary of the measurements made are listed in Table 3. Fig. 8 shows the DSC thermographs for all three materials. Allowing for instrument error, no differences in either the melting or crystallisation temperature for the polyamide-12 phase was obtained when either clay was added. There were slight differences in the enthalpies of melting (ΔH_m) and crystallisation (ΔH_c) between neat polyamide-12 and PA12-MAE, ΔH_m falling by 9% and ΔH_c reduced by 12% when MAE was added. The relative crystalline content in the composites was calculated, see Table 3, by assuming the ΔH_m for a theoretically 100% crystalline polyamide-12 to be 209.2 J/g [51] and allowing for the weight fraction of polymer in the composite. Additionally, during tensile testing a fibrous outer skin formed on the test piece. The crystalline content of the skin material and the bulk sample were similar, when measured by DSC. Both polyamide-12 and PA12-ME100 displayed one glass transition in their DSC curves. In contrast, the DSC trace of PA12-MAE showed two glass transition processes. The first was centred at 42 °C, the second a larger transition at about 80 °C. The latter transition had a larger specific heat capacity than the former, so we associate it with the glass transition of the amorphous polyamide-12 rich phase, shifted some 6–8 °C higher than that obtained for polyamide-12. The origin of the lower temperature T_g process may be from a phase derived from polyamide-12 clay interactions. The evolution of a similar lower temperaure T_g has recently been reported for a poly(9-vinyl

Table 3
Thermal Properties of PA12, PA12-ME100 and PA12-MAE

Thermal property	PA12	PA12-ME100	PA12-MAE
T_m [a] (°C)	173	172	173
T_c [b] (°C)	150	149	148
ΔH_m [c] (J/g)	32	31	29
ΔH_c [d] (J/g)	34	35	30
X_c [e] (%)	15.3	14.8	13.9
T_d [f] (°C)	485	485	495
CTE ($\times 10^{-6}$/°C)[g]	158	170	133

[a] Melting point from DSC second reheat at 10 °C/min.
[b] Crystallisation temperature measured on cooling at 10 °C/min.
[c] Enthalpy of melting, determined by DSC using heating rate of 10 °C/min.
[d] Enthalpy of crystallisation, determined by DSC applying a cooling rate of 10 °C/min.
[e] Relative crystalline content (%), calculated from DSC measurements.
[f] Decomposition temperature determined by TGA.
[g] Coefficient of thermal expansion from TMA measurements.

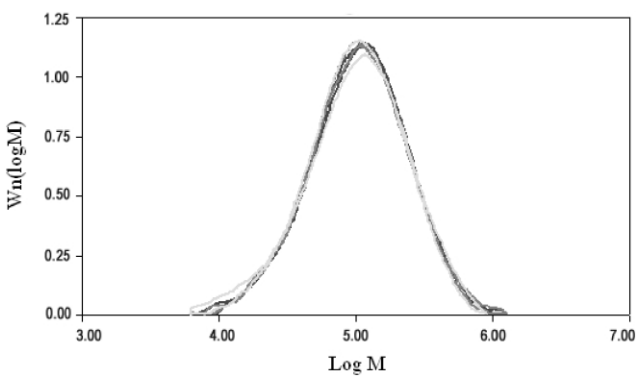

Fig. 7. Gel permeation chromatographs for PA12, PA12-ME100 and PA12-MAE.

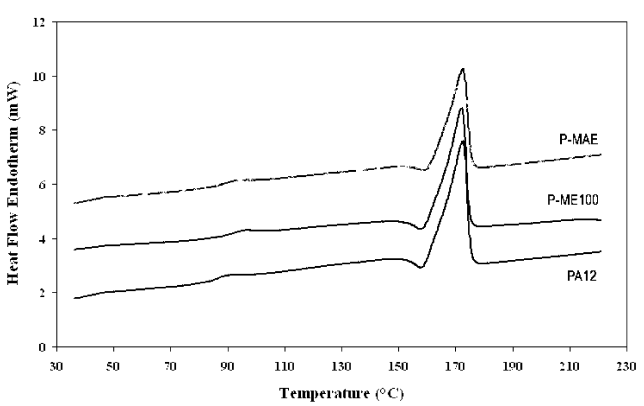

Fig. 8. DSC thermographs for PA12, PA12-ME100 and PA12-MAE.

carbazole) multi-walled carbon nanotube composite by Cadek et al. [52].

The coefficient of thermal expansion (CTE) for polyamide-12, PA12-ME100 and PA12-MAE was calculated from measurements made using thermal mechanical analysis. The CTE for PA12-ME100 increased by 8% compared to polyamide-12 itself while the presence of the modified MAE clay in the polymer reduced the CTE by 16%. The reduction in CTE for PA12-MAE is derived in part from the high aspect ratio of the predominately exfoliated silicate layers, compared to those poorly dispersed in PA12-ME100.

Fig. 9 shows the thermogravimetric analysis (TGA) as a function of temperature for (a) the two clays and (b) polyamide-12 and the composite materials. Fig. 9(a) clearly demonstrates the effect of the quaternary alkyl ammonium chloride modification of the clay surface has on the decomposition temperature (T_d) of the clays studied. The unmodified ME100 clay was thermally stable up to 540 °C, whereas the organically altered MAE clay started to decompose at 240 °C, some 300 °C below ME100. The drop in T_d was concomitant with a 40% weight loss. The decomposition temperatures for polyamide-12 and the composites are detailed in Table 3. The values for T_d obtained for polyamide-12 alone and PA12-ME100 after one and two passes in the melt blender were similar, typically 485 °C. The T_d of polyamide-12 was improved by 10 °C when MAE was added.

The dynamic mechanical properties of polyamide-12 itself and both composite materials were measured in the temperature range −100–100 °C over three decades of frequency. By way of example, we discuss the variation in tan δ and storage modulus (E') as a function of temperature at 1 Hz only, (see Fig. 10). Taking by convention the maximum in the tan δ peak at 1 Hz as a measure of the glass transition temperature (T_g), the T_g of polyamide-12 is at 10 °C. The T_g of PA12-ME100 is perhaps a couple of degrees higher, rising to about 30 °C for the PA12-MAE nanocomposite. While the absolute value of the T_g for the virgin polymer is slightly lower than that reported previously [53], the increase in T_g obtained particularly when the MAE clay was added may be associated with the confinement of the polymer chains in the interlayer spacing of the clay. This phenomenon connected with intercalated structures was evident from the XRD and microscopic results discussed above. The storage modulus or (dynamic flexural modulus) for polyamide-12 is shown in Fig. 10(b). Below −20 °C it is lower than that obtained for PA12-ME100. Above this temperature both polyamide-12 and PA12-ME100 had a similar profile. PA12-MAE on the other hand had a greater storage modulus over the entire temperature range examined. The enhancement of storage modulus of PA12-MAE results from strong interfacial interactions between the polymer and the clay platelets, the reduced mobility of polymer chains confined between or bonded to the clay surfaces and the inherent high modulus of

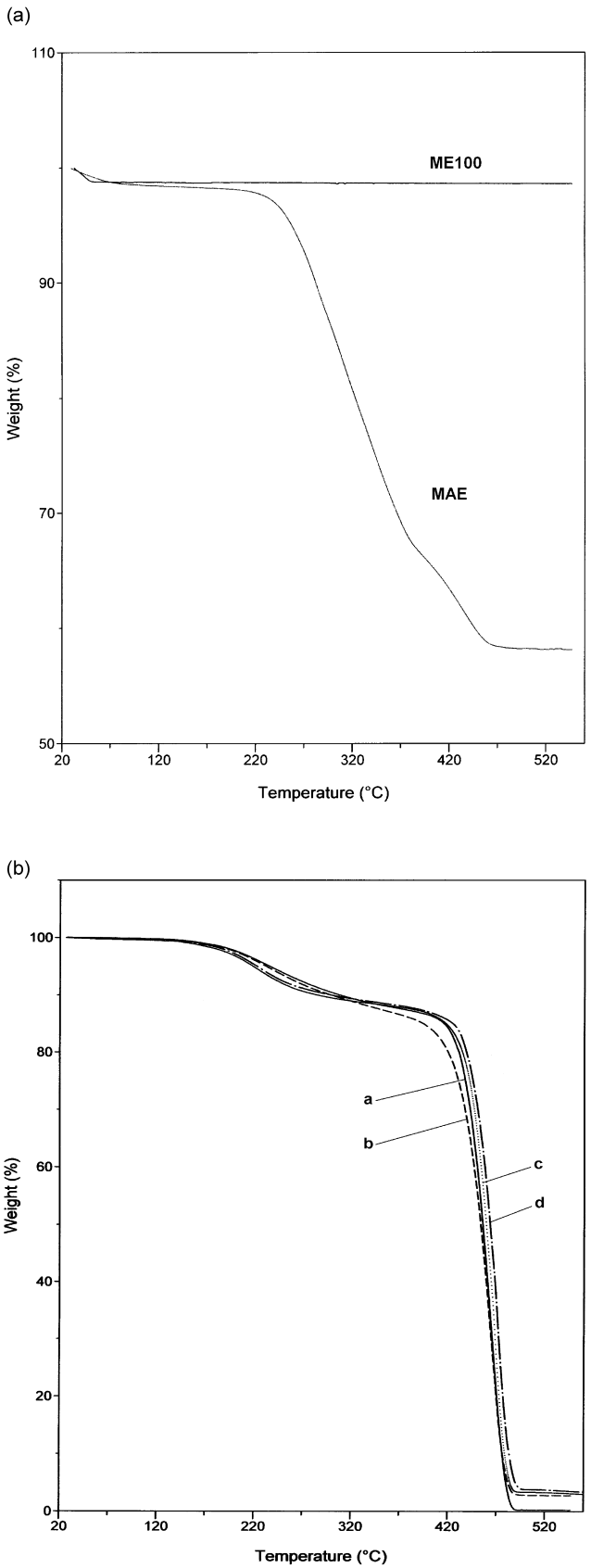

Fig. 9. Thermogravimetric decomposition curves for (a) both clays; ME100 and MAE, and (b) PA12, PA12-ME100 (first pass in extruder), PA12-ME100 (second pass in extruder) and PA12-MAE (second pass in extruder).

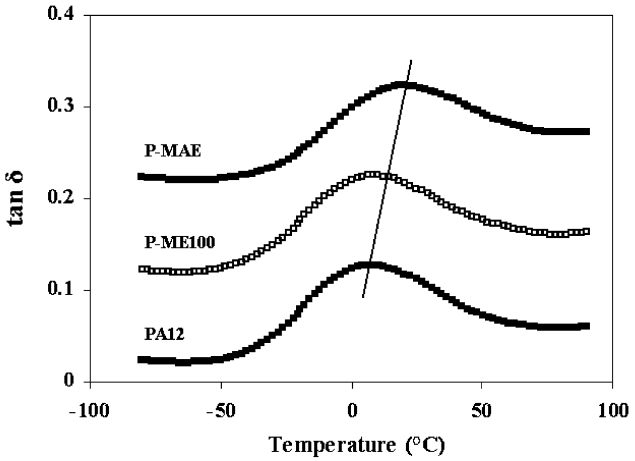

(a)

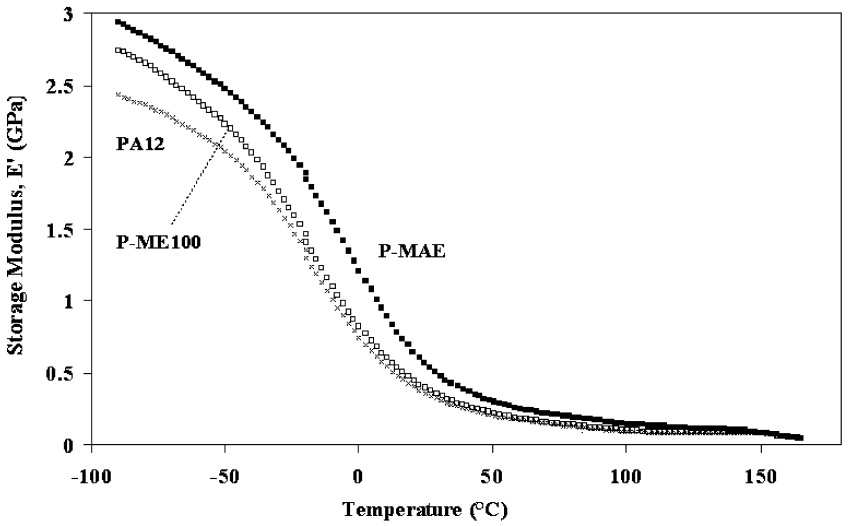

(b)

Fig. 10. Dynamic mechanical thermal analysis; variation in (a) tan δ and (b) storage modulus (E') as a function of temperature for PA12, PA12-ME100 and PA12-MAE measured at 1 Hz.

the clays. The activation energies (E_a) calculated using an Arrhenius type expression from data measured between 0.1 and 100 Hz. for polyamide-12 and PA12-ME100 were similar, typically 225 kJ/mol. However, E_a for PA12-MAE was higher, 271 kJ/mol., further evidence for interactions between the surface of the modified MAE clay and polyamide-12.

4. Conclusions

Polyamide-12/tetrasilisic fluoromica based nanocomposites were prepared using conventional single screw melt compounding. Both intercalated and exfoliated structures were detected and observed by XRD, SEM, TEM, HRTEM and AFM. HRTEM showed that the polyamide-12 crystallites lie perpendicular to the clay surface. The tensile modulus and strength of the PA12-MAE system were, respectively, 27 and 50% greater than that of neat polyamide-12. The flexural moduli of both nanocomposite materials were also higher than polyamide-12, a 50% enhancement in the case of PA12-MAE. An almost 3 fold increase in the elongation at break, from 180% to $>500\%$, was obtained when 4 wt% of quarternary tallow ammonium chloride modified fluoromica was blended with polyamide-12. The efficiency of this system to withstand large deformations is achieved by; (1) microvoid formation, which facilitates heat dissipation deformation mechanisms, (2) transfer of stresses between polymer and nanofiller and (3) by splitting, opening and slippage of clay layers. The

impact strength at room temperature of polyamide-12 and the composite materials was similar. However, the impact strength at −40 °C of PA12-ME100 fell by 47%, and that of PA12-MAE fell catastrophically, by up to 90%, when compared to neat polyamide-12. This dramatic fall in cold temperature impact strength may be a feature of highly exfoliated polymer nanocomposites, hitherto, not widely reported in the literature. The viscosity of the PA12-MAE was less than that of polyamide-12 alone over the entire shear rate range examined. Evidence from GPC measurements would suggest that the lower viscosity of the PA12-MAE system is associated with the slippage of polymer chains over clay layers in the molten state, and not with degradation or chain scission of the polymer chains during processing. The crystalline content of the PA12-MAE nanocomposite was less than neat polyamide-12 whether measured by XRD or DSC. The presence of the clays in the composite materials had no effect on either melting or crystallisation temperature of the polyamide-12 studied. The decomposition temperature of both polyamide-12 and PA12-ME100 were similar, and only an increase of 10 °C was achieved for PA12-MAE. The coefficient of thermal expansion increased slightly for PA12-ME100, but decreased by 16% for PA12-MAE. DMTA measurements showed an increase in the T_g of polyamide-12 on addition of the clays, by up to 15 °C for MAE, perhaps reflecting the confinement of polymer chains between clay stacks. The rise in T_g was concomitant with an increase in the storage modulus of the composite materials over polyamide-12, further evidence for polymer clay interactions.

Acknowledgements

This work was part funded by Teleflex Fluid Systems, Europe. The authors express their sincere thanks to Mr Yanai Shinichi and UNICOOP, Japan for their support and generous donation of SOMASIF clays. We also thank Dr Darren Martin, University of Queensland for helpful discussions.

References

[1] Carter LW, Hendricks JG, Bolley DS, US Patent 2,531,396, November, 1950.
[2] Fujiwara S, Sakamoto T. Japan Patent Application 109,998, September, 1976.
[3] Okada A, Fukushima Y, Kawasumi M, Inagaki S, Usuki A, Sugiyama S, Kurauchi T, Kamigaito O. US Patent 4,739,007, April, 1988.
[4] Usuki A, Kojima Y, Kawasumi M, Okada A, Fukushima Y, Kurauchi T, Kamigaito O. J Mater Res 1993;5:1179.
[5] Usuki A, Koiwai A, Kojima Y, Kawasumi M, Okada A, Kurauchi T, Kamigaito O. J Appl Polym Sci 1995;55:119.
[6] Pinnavaia TJ. Science 1983;220:365.
[7] Bleam WF, Hoffman R. Inorg Chem 1988;27:3180.
[8] Bleam WF, Hoffman R. Phys Chem Miner 1988;15:398.
[9] Vaia RA, Giannelis EP. Macromolecules 1997;30:7990.
[10] Vaia RA, Giannelis EP. Macromolecules 1997;30:8000.
[11] Whittingham MS, Jacobson AJ, editors. Intercalation chemistry. New York: Academic Press; 1992.
[12] Pinnavaia TJ. In: Legrand AP, Flandrois S, editors. Chemical physics of intercalation. New York: Plenum Press; 1987.
[13] Schöllhorn R. Physica 1990;99B:89.
[14] Theng BKG. The chemistry of clay organic. New York: Wiley; 1974.
[15] Theng BKG. Formation and properties of clay polymer complexes. New York: Elsevier; 1979.
[16] Mehrotra V, Giannelis EP. Solid State Commun 1991;77:55.
[17] Aranda P, Ruiz-Hitzky E. Adv Mater 1990;2:545.
[18] Greenland DJ. J Colloid Sci 1963;18:647.
[19] Zhao X, Urano K, Ogasawara S. Colloid Polym Sci 1989;267:899.
[20] Parfitt RL, Greenland DJ. Clay Miner 1970;8:305.
[21] Billingham J, Breen C, Yarwood J. Vibr Spectrosc 1997;14:19.
[22] Lan T, Pinnavaia TJ. Chem Mater 1994;6:2216.
[23] Wu J, Lerner MM. Chem Mater 1993;5:835.
[24] Jeon HG, Jung H-T, Lee SW, Hudson SD. Polym Bull 1998;41:107.
[25] Wang Z, Pinnavaia TJ. Chem Mater 1998;10:1820.
[26] Messersmith PB, Giannelis EP. J Polym Sci, Part A, Polym Chem 1995;33:1047.
[27] Messersmith PB, Giannelis EP. Chem Mater 1994;6:1719.
[28] Akelah A, Moet A. J Mater Sci 1996;31:3589.
[29] Zeng C, Lee LJ. Macromolecules 2001;34:4098.
[30] Huang X, Brittain WJ. Macromolecules 2001;34:3255.
[31] Choi YS, Choi MH, Wang KH, Kim SO, Kim YK, Chung IJ. Macromolecules 2001;34:8978.
[32] Vaia RA, Ishii H, Giannelis EP. Chem Mater 1993;5:1694.
[33] Vaia RA, Giannelis EP. Macromolecules 1997;30:8000.
[34] Kato M, Usuki A, Okada O. J Appl Polym Sci 1997;66:1781.
[35] Gelfer MY, Burger C, Hsiao BS, Chu B, Song HH, Avila-Orta CA, Liu L, Yeh F, Si M, Rafailovich M, Tsou AH. ACS Polym Prepr 2001; 42(2):79.
[36] Laus M, Francesangeli O, Sandrolini F. J Mater Res 1997;12:3134.
[37] Burnside SD, Giannelis EP. Chem Mater 1995;7:1597.
[38] Okada A, Usuki A. Mater Sci Engng 1995;C3:109.
[39] Heinemann J, Reichert P, Thomann R, Mülhaupt R. Macromol Rapid Commun 1999;20:423.
[40] Kawasumi M, Hasegawa N, Kato M, Usuki A, Okada A. Macromolecules 1997;30:6333.
[41] Reichert P, Nitz H, Klinke S, Brandsch R, Thomann R, Mülhaupt R. Macromol Mater Engng 2000;275:8.
[42] Fornes TD, Yoon PJ, Keskkula H, Paul DR. Polymer 2001;42:9929.
[43] Ray SS, Maiti P, Okamoto M, Yamada K, Ueda K. Macromolecules 2002;35:3104.
[44] Weber G, Kuntze D, Stix W. Colloid Polym Sci 1982;260:956.
[45] Bagely EB. J Appl Phys 1957;28:624.
[46] Reichert P, Kressler J, Thomann R, Müllhaupt R, Stöppelmann G. Acta Polym 1998;49:116.
[47] Kim G-H, Lee D-H, Hoffmann B, Kressler J, Stöppelmann G. Polymer 2001;42:1095.
[48] Cojazzi G, Fichera A, Garbuglio C, Malta V, Zannetti R. Makromol Chem 1976;168:289.
[49] Northolt MG, Tabor BJ, van Aartsen JJ. Progr Colloid Polym Sci 1975;57:225.
[50] Cho JW, Paul DR. Polymer 2001;42:1083.
[51] Gogolewski S, Czerniawska K, Gasiorek M. Colloid Polym Sci 1980; 258:1130.
[52] Cadek M, Coleman JN, Barron V, Hedicke K, Blau WJ. Appl Phys Lett 2002;81:5123.
[53] Aharoni SM. *n*-Nylons: their synthesis, structure and properties. New York: Wiley; 2001.